Nuclear envelope alterations generate an aging-like epigenetic pattern in mice deficient in Zmpste24 metalloprotease

Fernando G. Osorio,[1] Ignacio Varela,[1] Ester Lara,[2] Xose S. Puente,[1] Jesús Espada,[3] Raffaella Santoro,[4] José M. P. Freije,[1] Mario F. Fraga[5] and Carlos López-Otín[1]

[1]Departamento de Bioquímica y Biología Molecular and [2]Unidad de Epigenética, Instituto Universitario de Oncología, Universidad de Oviedo, 33006-Oviedo, Spain
[3]Instituto de Investigaciones Biomédicas ''Alberto Sols'', Consejo Superior de Investigaciones Científicas-Universidad Autónoma de Madrid, 28029-Madrid, Spain
[4]Institute of Veterinary Biochemistry and Molecular Biology, University of Zürich, Winterthurerstrasse 190, Zürich 8057, Switzerland
[5]Centro Nacional de Biotecnología, Consejo Superior de Investigaciones Científicas-Universidad Autónoma de Madrid, 28029-Madrid, Spain

Summary

Mutations in the nuclear envelope protein lamin A or in its processing protease ZMPSTE24 cause human accelerated aging syndromes, including Hutchinson–Gilford progeria syndrome. Similarly, *Zmpste24*-deficient mice accumulate unprocessed prelamin A and develop multiple progeroid symptoms, thus representing a valuable animal model for the study of these syndromes. *Zmpste24*-deficient mice also show marked transcriptional alterations associated with chromatin disorganization, but the molecular links between both processes are unknown. We report herein that *Zmpste24*-deficient mice show a hypermethylation of rDNA that reduces the transcription of ribosomal genes, being this reduction reversible upon treatment with DNA methyltransferase inhibitors. This alteration has been previously described during physiological aging in rodents, suggesting its potential role in the development of the progeroid phenotypes. We also show that *Zmpste24*-deficient mice present global hypoacetylation of histones H2B and H4. By using a combination of RNA sequencing and chromatin immuno-precipitation assays, we demonstrate that these histone modifications are associated with changes in the expression of several genes involved in the control of cell proliferation and metabolic processes, which may contribute to the plethora of progeroid symptoms exhibited by *Zmpste24*-deficient mice. The identification of these altered genes may help to clarify the molecular mechanisms underlying aging and progeroid syndromes as well as to define new targets for the treatment of these dramatic diseases.

Key words: aging; histone acetylation; lamina; methylation; progeria; proteolysis.

Correspondence

Carlos López-Otín, Departamento de Bioquímica y Biología Molecular, Facultad de Medicina, Universidad de Oviedo, 33006-Oviedo, Spain. Tel.: +34 985104201; fax: +34 985103564; e-mail: clo@uniovi.es Or Mario F. Fraga, Centro Nacional de Biotecnología, CSIC, Universidad Autónoma, 28029-Madrid, Spain. Tel.: +34 985109475; fax: +34 985109495; e-mail: mffraga@cnb.csic.es

FGO and IV have contributed equally to this work.

Introduction

Hutchinson–Gilford progeria syndrome (HGPS) is an accelerated aging process characterized by short stature, low body weight, early hair loss, lack of subcutaneous fat, scleroderma, decreased joint mobility, osteolysis, atherosclerosis, and premature death (Hennekam, 2006; Merideth *et al.*, 2008). Hutchinson–Gilford progeria syndrome belongs to an array of human disorders collectively known as laminopathies, caused by defects in components of the nuclear lamina and including Emery-Dreifuss muscular dystrophy, limb-girdle muscular dystrophy, dilated cardiomyopathy, Charcot-Marie-Tooth disease, Dunningan-type familial partial lipodystrophy, and mandibuloacral dysplasia (Navarro *et al.*, 2006; Ramirez *et al.*, 2007). Around 80% of patients with HGPS have the same de novo silent point mutation (G608G: GGC->GGT) in exon 11 of *LMNA* gene that encodes lamins A and C. This mutation activates a cryptic donor splice site, eliminating 150 bp of exon 11 and generating a truncated lamin A isoform known as progerin/LAdelta50 (De Sandre-Giovannoli *et al.*, 2003; Eriksson *et al.*, 2003).

Lamin A post-translational processing includes prenylation, cleavage of the C-terminal tripeptide, methylation of the prenylated C-terminal cysteine residue, and finally, the proteolytic removal of the C-terminal prenylated peptide by the metalloproteinase FACE-1/ZMPSTE24 (Pendas *et al.*, 2002). The target sequence of this last proteolytic event is included in the region deleted in progerin, and consequently progerin undergoes normally the initial steps of lamin A maturation but the prenylated peptide cannot be excised. Thus, the HGPS mutation causes the accumulation of permanently prenylated progerin, which leads to structural alterations in the nuclear envelope and its associated chromatin (De Sandre-Giovannoli *et al.*, 2003; Eriksson *et al.*, 2003). Similarly, disruption of the

murine *Zmpste24* gene prevents the cleavage of the lamin A prenylated peptide, leading to the accumulation of farnesylated prelamin A in the nuclear envelope. Prelamin accumulation in *Zmpste24*-deficient mice causes nuclear architecture abnormalities, shortened lifespan, and a progeroid phenotype that recapitulates most HGPS symptoms (Bergo *et al.*, 2002; Pendas *et al.*, 2002). Consequently, *Zmpste24*-deficient mice constitute a valuable animal model to study the mechanisms underlying the development of progeroid syndromes and to investigate possible therapeutic approaches for these pathologies. The transcriptional profiles of *Zmpste24*-deficient tissues and HGPS cells have been investigated, leading to the identification of signaling alterations that could be implicated in the onset of the progeroid phenotypes (Csoka *et al.*, 2004; Varela *et al.*, 2005; Osorio *et al.*, 2009). Significantly, the production of progerin, accompanied by some of these transcriptional alterations, has been detected in the context of physiological aging (Scaffidi & Misteli, 2006). These findings support the use of progeroid animal models such as *Zmpste24*-deficient mice to investigate the molecular mechanisms underlying the manifestations of normal and pathological aging. Nevertheless, despite the intense research in this field, little is known about the link between the alterations in nuclear structure and dynamics and the transcriptional deregulation detected in laminopathies. As nuclear structure is essential for a correct epigenetic pattern and because anomalous epigenetic signaling could be an important determinant of cellular senescence and organism aging (Issa, 2003; Sinclair & Oberdoerffer, 2009; Gravina & Vijg, 2010), we hypothesized that epigenetic alterations could be involved in the development of HGPS symptoms. In agreement with this hypothesis, changes in the methylation pattern of histone H3 have been recently described in HGPS cells but the relevance of these changes remains largely unknown (Scaffidi & Misteli, 2005; Shumaker *et al.*, 2006; Dechat *et al.*, 2008).

In the present work, we describe that the abnormalities in nuclear structure and dynamics caused by *Zmpste24*-deficiency lead to the accumulation of characteristic epigenetic marks such as rDNA hypermethylation and histone hypoacetylation. Based on these findings, together with the observation that similar abnormalities also occur during physiological aging, we propose that chromatin disorganization generates a characteristic aging-like epigenetic pattern which contributes to the transcriptional deregulation associated with both normal and accelerated aging.

Results

Zmpste24-deficiency causes hypermethylation of ribosomal DNA

DNA methylation and histone post-translational modifications are the most widely analyzed epigenetic changes. The relationship between DNA methylation and aging is complex. Early studies suggested the occurrence of a global decrease in DNA methylation associated with physiological aging (Wilson &

Jones, 1983). By contrast, other works have revealed that an overall decrease in DNA methylation is not a common feature of mammalian aging, and changes in this regard are circumscribed to a specific subset of genes (Tawa *et al.*, 1992; Tra *et al.*, 2002; Fuke *et al.*, 2004). Further studies have even shown that several loci in CpG islands gain methylation with age (Christensen *et al.*, 2009; Maegawa *et al.*, 2010). To evaluate the putative occurrence of DNA-methylation alterations in *Zmpste24*$^{-/-}$ progeroid mice, we first analyzed by high-performance capillary electrophoresis (HPCE) the global 5-methylcytosine (5mC) content in liver samples from these mutant mice. As shown in Fig. 1a, we did not observe significant differences in global methylation between *Zmpste24*$^{-/-}$ and control mice. Likewise, we failed to find significant methylation differences in subtelomeric regions or in major satellites located in pericentromeric regions of DNA from *Zmpste24*$^{-/-}$ mice when compared with wild-type animals (Fig. 1b).

To test the possibility that specific alterations in the methylation status of certain DNA loci rather than global changes in DNA methylation, could be linked to the premature aging of *Zmpste24*$^{-/-}$ mice, we investigated the methylation pattern of their ribosomal RNA-encoding genomic regions (rDNA), as several works have shown that alterations in rDNA methylation occur in aging (Johnson *et al.*, 1998; Olson & Dundr, 2005). Ribosomal RNA is synthesized as a 45S pre-rRNA, which is subsequently processed into 18S, 5.8S, 28S, and 5S mature rRNAs. Interestingly, and as can be seen in Fig. 2, bisulfite sequencing analysis revealed a significant trend to hypermethylation of the rDNA units of *Zmpste24*$^{-/-}$ mice, especially in internal regions such as the 28S 5′-region. Remarkably, two CpG sites located at positions -133 and -144 in the Upstream Control Element (UCE) of the rDNA promoter are hypermethylated in *Zmpste24*-deficient animals (Fig. 2). Methylation of these two CpGs is sufficient to inhibit the formation of the Pol I pre-initiation complex, thus blocking rDNA transcription (Chen & Pikaard, 1997; Santoro *et al.*, 2002). Consistent with these results, qRT–PCR experiments revealed a significant reduction in 45S pre-rRNA in *Zmpste24*-deficient animals, which was reverted upon azacitidine treatment (Fig. 3a), providing additional support to the causal role of promoter hypermethylation in this alteration. We next used chromatin immunoprecipitation to examine the amounts of rDNA-associated RNA polymerase I. As shown in Fig. 3b, while the levels of polymerase bound to the promoter region are similar among wild-type and mutant animals, *Zmpste24*$^{-/-}$ mice show a 3-fold reduction in the levels of elongating RNA polymerase I associated with the rDNA coding regions. Collectively, these results indicate that *Zmpste24* deficiency causes a severe dysfunction of rRNA gene activity, which could be implicated in the premature cellular senescence and accelerated aging phenotype observed in these mice (Varela *et al.*, 2005). In agreement with this possibility, rDNA hypermethylation has been reported to occur during physiological aging in rats (Oakes *et al.*, 2003), and a decrease in the rRNA gene activity with age has also been observed in humans (Thomas & Mukherjee, 1996).

Loss of acetylated forms of nucleosome histones in *Zmpste24*$^{-/-}$ mice

Chromatin conformation and transcriptional control are influenced not only by promoter methylation but also by histone post-translational modifications, most notably site-specific methylation and acetylation/deacetylation of histone tails (Shahbazian & Grunstein, 2007). Interestingly, genes potentially involved in the progeroid phenotype of *Zmpste24*-deficient mice, such as p21WAF1 and INK4/ARF, have been described to be regulated by histone acetylation (Archer *et al.*, 1998; Matheu *et al.*, 2005). Consequently, we decided to investigate the modification status of histones in *Zmpste24*-deficient mice. As a first approach to this aim, we used HPCE to analyze H2B and H4 acetylation status. As can be seen in Fig. 4a, *Zmpste24*-deficient mice show a loss of about 15% of global acetylation in histone H4, produced by a reduction in all its monoacetylated, diacety-

lated, and triacetylated forms. Likewise, and similar to the case of histone H4, *Zmpste24*-deficient mice show an important decrease (about 50%) in global acetylation of histone H2B (Fig. 4b). This decrease mainly derives from a significant loss (about 80%) of the monoacetylated form of H2B. To determine the residue that could be target of this specific loss of acetylation, we carried out mass spectrometry analysis on this fraction. As can be seen in Fig. 5a, we observed a clear decrease in the relative abundance of a peptide corresponding to the first 12 amino acids of the protein which contain one acetyl group at lysine 5, indicating that the loss of H2B monoacetylation occurs mostly at this residue. This conclusion was further confirmed by Western blot analysis with an antibody that specifically recognizes this modification (Fig. 5b). This analysis also showed that this decrease in histone acetylation is not restricted to the liver. As can be seen in Fig. 5b, the same alteration was also present in other tissues from *Zmpste24*-deficient mice.
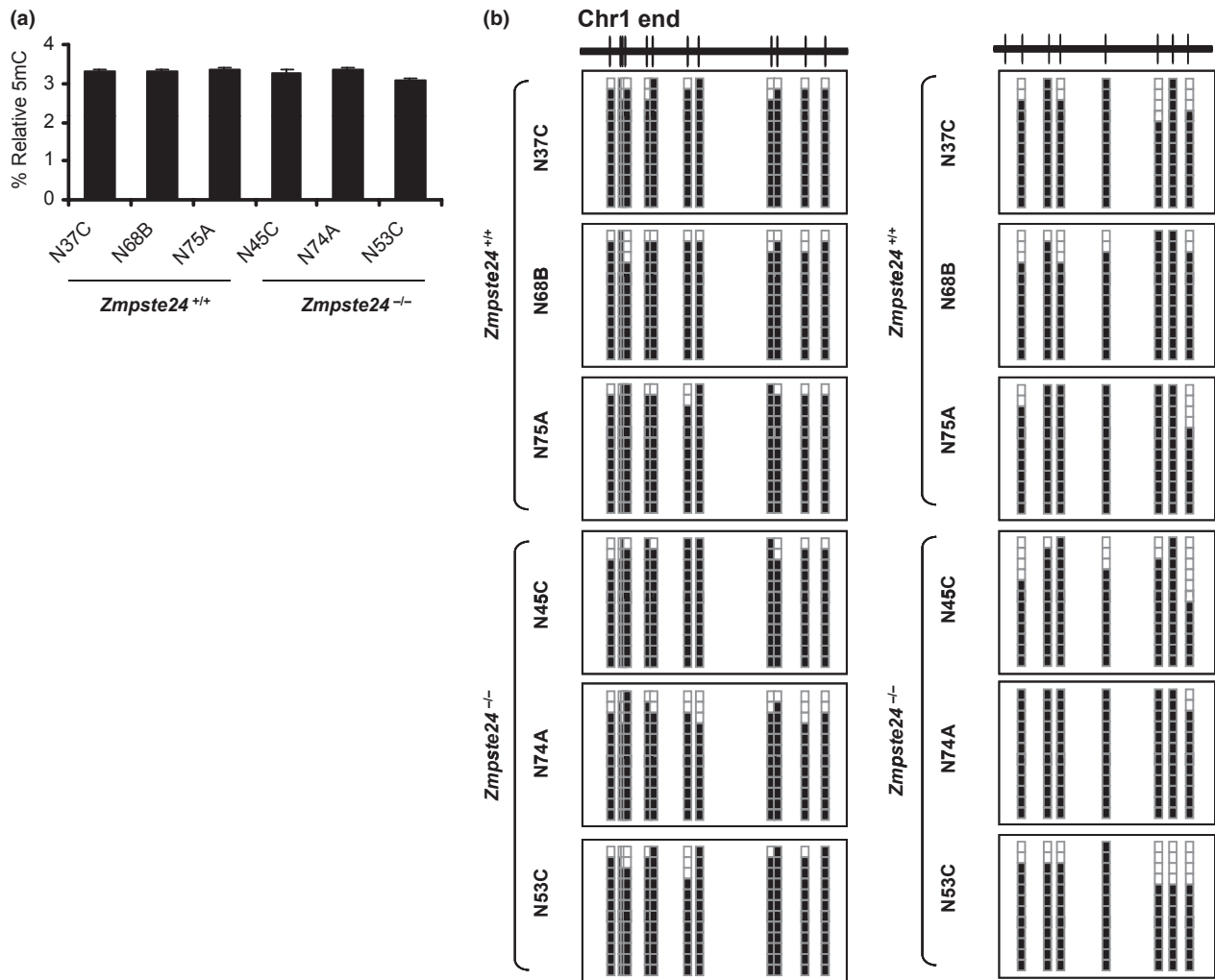

Fig. 1 Global DNA methylation analysis in *Zmpste24*$^{-/-}$ mice. (a) Global 5-methyl-cytosine content analyzed by high-performance capillary electrophoresis (HPCE) in liver samples from representative wild-type (N37C, N68B, and N75A) and *Zmpste24*-deficient mice (N45C, N74A, and N53C). (b) Analysis of the DNA methylation status by bisulfite sequencing of multiple clones (see Experimental procedures) of subtelomeric repeats (left) and major satellites (right) in liver samples from the same control and *Zmpste24*$^{-/-}$ mice as in (a). Distribution of CpG sites within the amplified DNA is shown by vertical bars on and horizontal bar over each panel. Three mice per genotype and 12 clones per mouse were analyzed. Methylated and unmethylated CpG positions are shown as black and white squares, respectively.
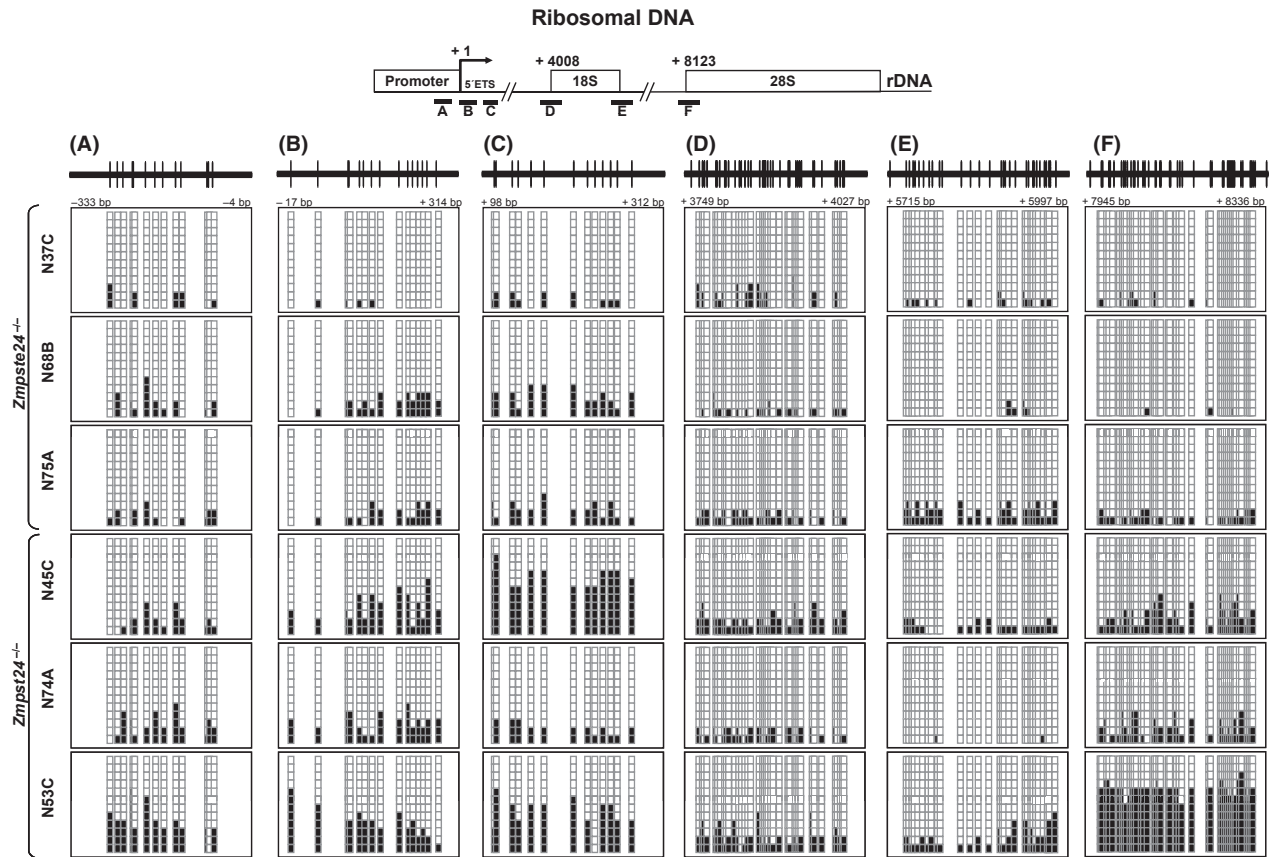
Fig. 2 rDNA methylation analysis in *Zmpste24*⁻/⁻ mice. Analysis of DNA methylation at ribosomic DNA using bisulfite sequencing of multiple clones in liver DNA samples from *Zmpste24*-deficient mice (N45C, N74A and N53C) and control littermates (N37C, N68B and N75A). Scheme showing the rRNA gene (top), depicting the six regions subjected to methylation analysis (AF); these correspond to the proximal promoter (A-C), and the ends of 18S (D-E) and 28S (F) regions. Three mice per genotype and twelve clones per mouse were analyzed. Methylated and unmethylated CpG positions are represented as black and white squares, respectively.
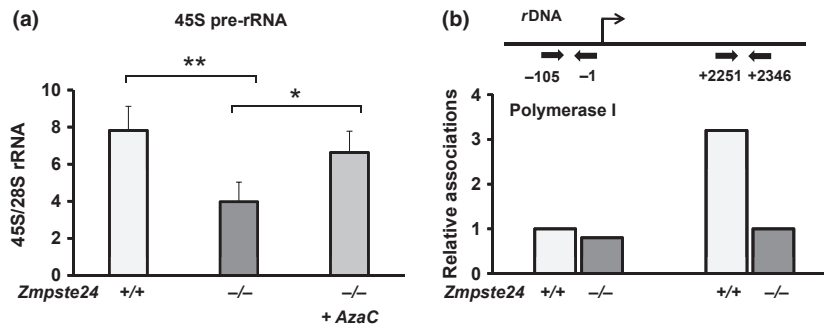

Fig. 3 Transcriptional activity of the rRNA gene in *Zmpste24*⁻/⁻ mice. (a) qRT–PCR quantification of the precursor rRNA transcript in liver samples from wild-type, *Zmpste24*-deficient animals, and azacitidine-treated *Zmpste24*-deficient mice (AzaC) relative to the levels of 28S rRNA. (b) RNA polymerase I association with the rDNA promoter and internal regions indicated at the top, as determined by chromatin immunoprecipitation of liver samples from *Zmpste24*⁻/⁻ mice and control littermates. A schematic map of the rRNA gene is included at the top, indicating the position of the two analyzed regions. *$P < 0.05$. Error bars represent SEM.

Acetyl-H2B-mediated differential gene regulation in *Zmpste24*⁻/⁻ mice

The reduction of acetylated forms of nucleosome histones is associated with a stronger association of these nucleosomes with the DNA, which generates a more compacted or silent chromatin state. We hypothesized that the decrease of histone acetylation observed in *Zmpste24*⁻/⁻ mice could produce both a general decrease in the transcriptional activity of their cells and a deregulation of the expression of specific genes implicated in the generation of the senescence phenotype observed in these animals. Consequently, we performed two independent ChIP-
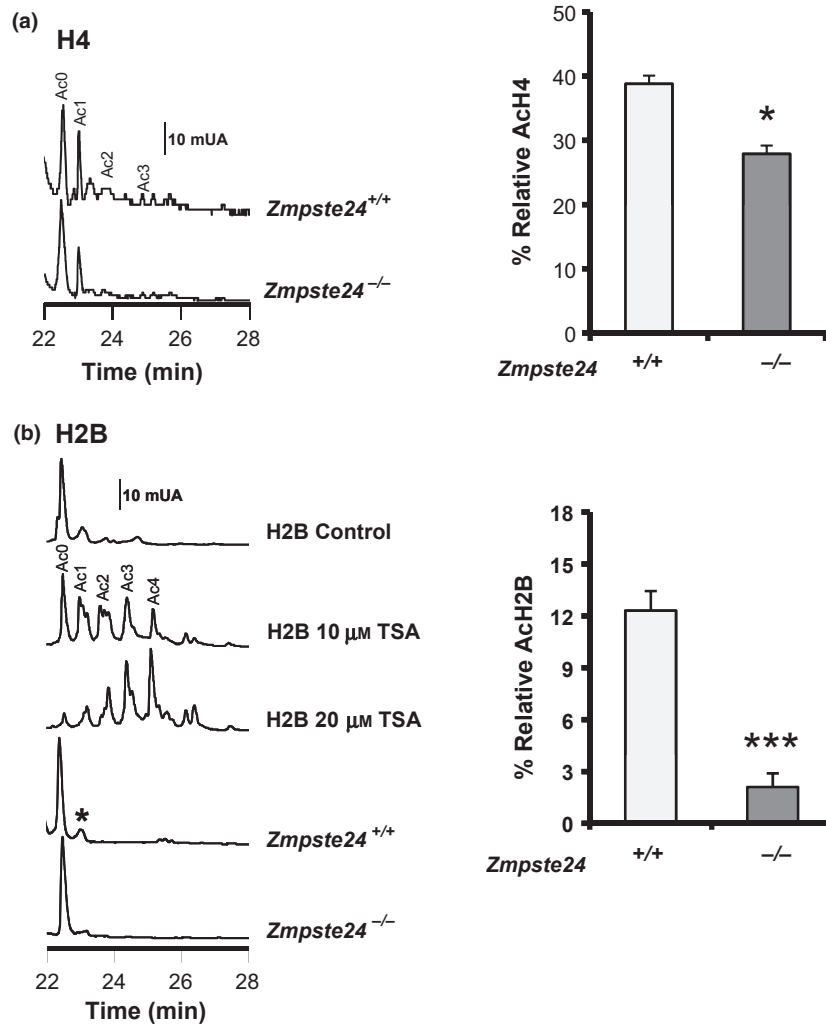
Fig. 4 Histones H4 and H2B acetylation status in *Zmpste24*$^{-/-}$ mice. (a) High-performance capillary electrophoresis (HPCE) analysis of histone H4 post-translational modifications. Representative electropherograms show peaks corresponding to the nonacetylated (Ac0), mono- (Ac1), di- (Ac2), and triacetylated (Ac3) forms of histone H4 in liver samples from wild-type (WT) and *Zmpste24*-deficient mice (left). Relative levels of acetylated histone H4 in two WT and three mutant mice (right). (b) HPCE analysis of histone H2B post-translational modifications. Representative electropherograms corresponding to liver samples from WT and *Zmpste24*-deficient mice are shown, along with samples from HL60 cells treated with the indicated concentrations of the histone deacetylase inhibitor trichostatin A (TSA) (left). Electropherograms of samples treated with TSA show mono-, di-, tri-, and tetra-acetylated forms of histone H2B. Relative levels of acetylated histone H2B in three WT and three mutant mice (right) are shown. *$P < 0.05$; ***$P < 0.001$. Error bars represent SEM.

on-Chip experiments to determine specific genomic regions of association of acetyl-H2B in both *Zmpste24*$^{-/-}$ and control mice. In the first experiment, we compared samples from a *Zmpste24*$^{-/-}$ mice with a control littermate, while for the second experiment we used pools of genomic DNA obtained from three wild-type and three mutant animals, respectively. A complete list of all the probes that showed recurrent differences in enrichment between *Zmpste24*-deficient and control samples can be found in Tables S2 and S3 (Supporting information). Additionally, and to determine if the putative differences in association of acetyl-H2B to specific genomic regions of control and mutant mice could modulate the expression of specific genes, we performed transcriptional profiling on liver samples from a *Zmpste24*$^{-/-}$ mouse and a littermate control. For this purpose, we isolated total liver RNA and used it for expression analysis by

ultra-deep RNA sequencing using an Illumina platform (Wilhelm *et al.*, 2008).

A list of key genes that were found recurrently enriched in the samples belonging to control mice compared to *Zmpste24*$^{-/-}$ mice and which also showed a reduced expression in *Zmpste24*-mutant samples is shown in Table 1. Additional validation of these results was performed by qRT–PCR, as shown in Fig. S1 (Supporting information). Interestingly, one of these genes is *Bcl6*, a known inhibitor of the senescence process mediated by p53 (Shvarts *et al.*, 2002). The transcriptional down-regulation of this gene can play a key role in the accelerated senescence phenotype triggered by the activation of p53 observed in *Zmpste24*-deficient mice. We also observed transcriptional down-regulation associated with a decrease in the levels of acetyl-H2B in several genes involved in fatty acid metabolism (*Sec14p*,
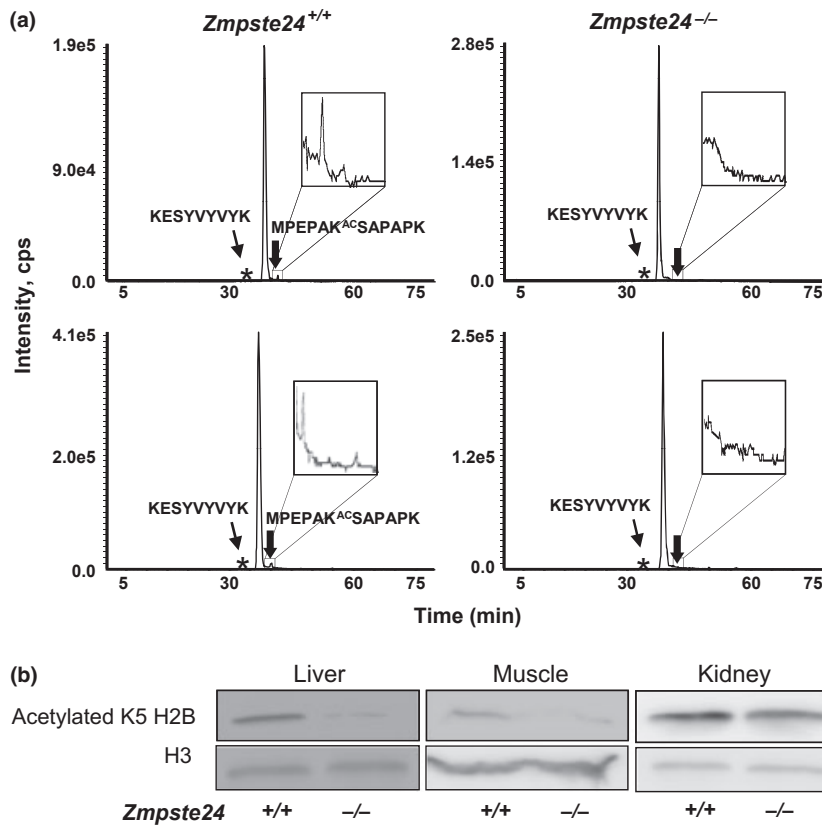
Fig. 5 H2B acetylation in lysine 5 in *Zmpste24*$^{-/-}$ mice. (a) Mass spectrometry identification of the histone H2B residue differentially acetylated in wild-type vs. *Zmpste24*$^{-/-}$ mice. Identification of the peptide MPEPACK^{AC}SAPAPK indicates the presence of acetylated histone H2B at lysine 5 in control samples (left); this peptide is not detected in *Zmpste24*$^{-/-}$ mice (right). Control peptide is shown (*). (b) Western blot analysis of histone H2B acetylation in control and *Zmpste24*-deficient. Histone H3 was used as a loading control.

Table 1 Genes recurrently enriched in either *Zmpste24*$^{+/+}$ (upper half) or *Zmpste24*$^{-/-}$ (lower half) samples that also show changes in expression levels

Gene	ChIP on chip Analysis		Expression Analysis	
	Enrichment	P-value	*Zmpste24*$^{-/-}$	*Zmpste24*$^{+/+}$
Elovl3	2.399	0.011	0.38	335.02
Cmah	2.188	0.012	0.28	1.82
Ifi47	2.117	0.003	1.94	5.17
6430527G18Rik	2.100	0.011	1.02	2.37
Sec14l2	2.044	0.009	20.69	88.66
Bcl6	1.895	0.002	3.56	6.87
Apoc1	1.689	0.006	2639.22	6902.38
Ppp1r3b	1.622	0.005	3.27	21.41
Cyp2b10	3.579	0.026	70.84	0.11
Fmo2	3.293	0.014	1.75	0.23
Apcs	3.278	0.007	803.57	71.87
Htatip2	2.775	0.009	31.87	5.11
Cyp4a14	2.684	0.019	65.31	5.02
Fgl1	2.554	0.009	1007.95	119.41
Agxt2l1	2.162	0.012	114.41	6.16
Orm1	2.111	0.007	4201.28	528.02

The enrichment value refers to the ratio between the enrichment ratios obtained in *Zmpste24*-deficient and control samples. Control vs. *Zmpste24*$^{-/-}$ in the upper half and *Zmpste24*$^{-/-}$ vs. control in the lower half.

Elovl3, and *Apoc1*) and glycogen metabolism (*Ppp1r3b* and *Cmah*). These alterations may contribute to the lipodystrophy phenotype and the altered metabolic response previously described in *Zmpste24*$^{-/-}$ mice (Pendas *et al.*, 2002; Marino *et al.*, 2008).

In addition to this general decrease in acetylation of the histone H2B, we could also observe specific enrichment of acetyl-H2B in several genes from *Zmpste24*-deficient samples. Some of them are also transcriptionally up-regulated in these progeroid mice. Remarkably, among these genes we have found *Apcs* (Table S3, Supporting information) that has been reported to control chromatin degradation and could be involved in the chromatin abnormalities observed in *Zmpste24*$^{-/-}$ cells (Bickerstaff *et al.*, 1999; Varela *et al.*, 2005). Additionally, we have also found acetyl-H2B-related up-regulation of known proliferation inhibitors such as *Agxt2l1* and *Htatip2* that could contribute to the senescence phenotype. Finally, several genes involved in liver inflammation and detoxification were identified (*Cyp2b10*, *Cyp4a14*, *Orm1*, *Fmo2*, and *Fgl1*). The up-regulation of these genes could indicate that the liver from *Zmpste24*-deficient mice is subjected to a kind of cellular stress that triggers an adaptive metabolic response involving the activation of inflammation and detoxification mechanisms in these progeroid mice.

Discussion

Hutchinson–Gilford progeria syndrome is a premature aging disease characterized by a rapid progression of symptoms such as hair loss, growth retardation, lack of subcutaneous fat, aged-looking skin, osteoporosis, and arteriosclerosis. Patients with HGPS usually die at around 13 years and there is no specific treatment for them (Navarro *et al.*, 2006). Accordingly, analysis of the molecular pathways implicated in the development of this disease has been necessary for developing therapeutic approaches for these patients (Espada *et al.*, 2008; Varela *et al.*, 2008). In this scenario, *Zmpste24*-deficient mice, which also accumulate a farnesylated lamin A precursor, have become an excellent tool for the molecular study of progeria. The use of these mice has allowed to demonstrate that the accumulation of farnesylated prelamin A causes alterations in nuclear structure and chromatin organization, which in turn activate DNA damage sensor pathways that finally lead to the development of the progeroid phenotypes characteristic of *Zmpste24*-mutant mice (Liu *et al.*, 2005; Varela *et al.*, 2005). Nevertheless, the molecular links between the chromatin disorganization and the transcriptional alterations present in these progeroid mice remain unknown. In this work, we report the presence of epigenetic alterations in *Zmpste24*-deficient mice which are related to those observed in physiologically aged mice. We also propose that these epigenetic abnormalities may be implicated in the development of the progeroid phenotype.

Previous studies have reported a significant decrease in global DNA methylation with aging (Wilson & Jones, 1983; Richardson, 2003; Fuke *et al.*, 2004). By contrast, this trend was not observed in our progeroid animal model, in which the total methylcytosine content did not differ significantly from that of control mice. These differences between methylation changes in physiological and accelerated aging could derive from the fact that the loss of global DNA methylation during physiological aging mainly results of the passive demethylation of heterochromatic DNA, because of a progressive loss of efficacy of DNA methyltransferase 1 (Dnmt1) or to the erroneous targeting of this enzyme by other cofactors (Casillas *et al.*, 2003). The shortened lifespan of *Zmpste24*-deficient mice, which develop an evident progeroid phenotype before the decline in Dnmt1 activity occurs, could contribute to explain the absence of global DNA demethylation in this animal model of accelerated aging. Nevertheless, it is remarkable that, in accordance with our observations in this progeroid animal model, a number of works have reported that an aging-associated decline in total methylcytosine content is not a common finding in mammalian tissues (Tawa *et al.*, 1992; Tra *et al.*, 2002; Fuke *et al.*, 2004). Furthermore, very recent studies have demonstrated that several loci present in CpG islands gain methylation with age (Christensen *et al.*, 2009; Maegawa *et al.*, 2010), pointing to the need of detailed analysis of specific genes in specific tissues before raising definitive conclusions about the relevance of methylation changes during normal and pathological aging.

Consistent with this possibility, and in contrast to the absence of alterations in global methylation, we observed a marked hypermethylation of the rDNA loci in *Zmpste24*−/− progeroid mice. This epigenetic mark has been previously described in physiological aging but its precise relevance in this process is largely unknown (Oakes *et al.*, 2003). Our observation that rDNA hypermethylation also occurs in the context of accelerated aging suggests that it could be functionally involved in the development of age-associated phenotypes and consequently it could provide a potential target of anti-progeroid therapies. We hypothesize that down-regulation of rDNA transcription resulting from promoter hypermethylation plays a crucial role in the cellular senescence phenotype observed in both accelerated and physiological aging. Supporting this proposal, it has been described that rDNA hypermethylation is associated with progression-free survival in ovarian and endometrial cancer (Powell *et al.*, 2002; Chan *et al.*, 2005).

In relation to histone modifications, we describe herein that *Zmpste24*-deficient mice present hypoacetylation of histones H2B and H4, which in the case of H2B mostly occurs in the monoacetylated form modified at lysine 5. Although the significance of this loss of acetylation is still unclear, the general trend to a loss of histone acetylation suggests a switch of chromatin structure to a close, inactive conformation, characteristic of quiescent or senescent cellular states, which could contribute to the cellular phenotype observed in these mice. Alternatively, histone modifications can promote specific promoter methylation and regulate DNA transcription even in the absence of methylation, as described in the case of *CDKN1A* locus (Archer *et al.*, 1998; Richon *et al.*, 2004). Finally, we have found a direct correlation between loss of acetylated forms of histone H2B and transcriptional down-regulation of several genes involved in the control of proliferation/senescence such as *Bcl6*, *Apcs*, or *Htatip2*, which can contribute to the senescence phenotype observed in the context of *Zmpste24* deficiency (Varela *et al.*, 2005, 2008). Additionally, the expression of other genes involved in fatty acid and glycogen metabolism is also altered and can contribute to the systemic defects described in *Zmpste24*−/− mice (Marino *et al.*, 2008). Also in this regard, we must emphasize that other histone modifications distinct from loss of H2B and H4 acetylation can also contribute to the multiple alterations observed in the *Zmpste24*−/− progeroid mice and further studies will be required to clarify this question. Nevertheless, the identification of a series of genes with marked expression changes associated with specific histone modifications in tissues from *Zmpste24*−/− mice may help to further clarify the molecular mechanisms underlying aging and progeroid syndromes and to define new targets for the treatment of these devastating diseases.

Experimental procedures

Animals

Face1/Zmpste24-deficient mice were generated and genotyped as described (Pendas *et al.*, 2002). For *in vivo* inhibition of DNA

methylation, 5-azacitidine (2 mg Kg^{-1} day^{-1}) in PBS was administrated intraperitoneally to mice every day for 1 week. Four month-old *Face1/Zmpste24*-deficient mice and littermate controls were sacrificed by cervical dislocation, and their livers were extracted and stored at −80°C until further use. All the procedures were carried out following the guidelines of the animal facility of the Universidad de Oviedo.

Analysis of sequence-specific DNA methylation

The methylation status of specific genomic DNA sequences was established by bisulfite genomic sequencing (Fraga *et al.*, 2005). Following the bisulfite conversion reaction, the DNA sequence was amplified by PCR with primers specific for the bisulfite-converted DNA. The PCR product was cloned and at least ten colonies per sequence were sequenced automatically to determine the methylation status of each sample. The percentage of methylation for each sample was calculated based on the number of clones that showed methylated or unmethylated cytosines. Primer sequences are available as Table S1 (Supporting information).

Quantification of global DNA methylation

5-Methylcytosine (5mC) genomic content was determined by HPCE, as described (Fraga *et al.*, 2002). Briefly, genomic DNA samples were boiled, treated with nuclease P1 (Sigma, St. Quentin Fallavier, France) for 16 h at 37°C and with alkaline phosphatase (Sigma, St. Quentin Fallavier, France) for an additional 2 h at 37°C. After hydrolysis, total cytosine and 5mC content were measured by HPCE using a P/ACE MDQ system (Beckman-Coulter, Beckman-Coulter, Fullerton, CA, USA). Cytosine and methylcytosine were separated and quantified using the sodium dodecylsulfate (SDS) micelle system, based on size, charge, structure, and hydrophobicity differences after the application of specific voltages using a narrow-bore fused silica capillary tube. Relative 5mC content was expressed as a percentage of total cytosine content (methylated and nonmethylated).

Quantification of histone acetylation

Histones were prepared in accordance with established protocols (Turner & Fellows, 1989) and global acetylation at histones H2B and H4 was quantified as previously described (Fraga *et al.*, 2005). Individual histone fractions were extracted from cell nuclei by acid treatment, and then purified by reverse-phase high performance liquid chromatography (HPLC) on a Jupiter C18 column (Phenomenex Inc., Torrance, CA, USA) with an acetonitrile gradient (20–60%) in 0.3% trifluoroacetic acid, using a HPLC gradient system (Beckman-Coulter). This method separates molecules based on their hydrophobicity. Samples were lyophilized and then dissolved in 5 mM DTT to avoid oxidation. Acetylated histone derivatives were resolved by HPCE as described (Fraga *et al.*, 2005). In brief, nonacetylated, mono-, di- and polyacetylated histone derivatives were resolved by

HPCE. An uncoated fused silica capillary (60.2 cm × 75 μm, effective length 50 cm; Beckman-Coulter) was used in a CE system (P/ACE MDQ; Beckman-Coulter) connected to a data-processing station (32 Karat Software; Beckman-Coulter). The running buffer was 100 mM phosphate buffer, pH 2.0 containing 0.02% (w/v) HPM-cellulose, and running conditions were 25°C with operating voltages of 12 kV. On-column absorbance was monitored at 214 nm. Before each run, the capillary system was conditioned by washing with 0.1 M NaOH (3 min), with 0.5 M H$_2$SO$_4$ (2 min), and equilibrated with running buffer (3 min). Samples were injected under pressure (0.3 psi, 3 s). All samples were analyzed in duplicate and three measurements were made per replicate.

Nano-liquid chromatography and tandem mass spectrometry

The resulting H2B-derived tryptic peptides from control and mutant samples were on line injected onto a C18 reversed-phase micro-column (300 mm ID × 5 mm PepMapTM; LC Packings, Amsterdam, The Netherlands) to remove salts, and then analyzed in a continuous acetonitrile gradient consisting of 0–50% B in 45 min and 50–90% B in 1 min (B = 95% acetonitrile, 0.5% acetic acid in water) on a C18 reversed-phase nano-column (100 mm ID × 15 cm, Discovery®; BIO Wide pore, Supelco, Bellafonte, PA, USA). A flow-rate of 300 nL min^{-1} was used to elute peptides from the reversed-phase nano-column to a PicoTip™ emitter nano-spray needle (New Objective, Woburn, MA, USA) for real-time ionization and peptide fragmentation on a 4000 Q-Trap LC/MS/MS system (Applied Biosystems/MDS Sciex, Concord, ON, Canada) equipped with a nanospray ion source (Protana, Ontario, Canada). Nano-liquid chromatography was automatically performed on an advanced nano-gradient generator (Ultimate nano-HPLC; LC Packings) coupled to an autosampler (Famos; LC Packings). The needle voltage was set at 3000 V. Nitrogen was used as curtain (value of 15) and collision gas (set to high). For the analysis, in the multiple reaction monitoring mode (MRM), Q1 was set on the multiply charged parent ions at the indicated *m/z* values. Q3 was set on the marker filtering signal selected for each parent ion. Collision energy was set to 20. All chromatograms and MS/MS spectra were analyzed by the software packages Analyst 1.4.1 (Applied Biosystems).

ChIP-on-Chip and data analysis

The chromatin immunoprecipitation assay was carried out as described (Fraga *et al.*, 2005) with anti-acK5H2b (Cell Signaling). DNA-protein interactions were fixed using formaldehyde as a crosslinking agent. Crosslinked protein/chromatin was fragmented by sonication into fragments of ~200–800 bp. Protein was then immunoprecipitated from the lysate using a specific antibody. After reversal of crosslinking, proteins were removed, DNA purified and used for ChIP-on-Chip assays. The ChIP on Chip assay was performed on the Agilent Mouse Promoter ChIP-on-chip microarrays with Designs IDs 014716 and 014717

containing probes covering 5.5 kb upstream and 2.5 kb downstream of the transcriptional start sites. Labeling was performed using a BioPrime Total Genomic Labelling System (Invitrogen, Carlsbad, CA, USA) following manufacturer instructions. The hybridization was performed following Agilent manual G4481-90010. The arrays were scanned on a G2565BA DNA microarray scanner (Agilent) and the images were quantified using Agilent Feature Extraction Software v9.5.3. Finally, Agilent ChIP Analytics v1.3.1 was used as analysis software using Whitehead model v1.0 as error model.

RNA sequencing

Transcriptional profiling of livers from *Zmpste24*-deficient and control mice was performed by RNA sequencing. Briefly, total RNA was used for cDNA synthesis and sequenced at The Centre for Applied Genomics, The Hospital for Sick Children, Toronto, Canada, using a GAII instrument following the manufacturer instructions (Illumina). Reads were mapped to the mouse reference genome (mm9) using TopHat and Bowtie (Trapnell *et al.*, 2009), and gene expression was computed using Cufflinks (Trapnell *et al.*, 2010) and mouse gene models from Ensembl v56. Relative expression was expressed as RPKM values (Reads Per Kilobase of transcript per Million mapped reads).

Western blotting

Mice tissues were immediately frozen in liquid nitrogen after extraction and were homogenized in a 20 mM Tris buffer pH 7.4, containing 150 mM NaCl, 1% Triton X-100, 10 mM EDTA, and Complete® protease inhibitor cocktail (Roche Applied Science, Indianapolis, IN, USA). Once homogenized, tissue extracts were centrifuged at 12 000 *g* at 4°C and supernatants were collected. The protein concentration of the supernatant was evaluated by bicinchoninic acid technique (BCA protein assay kit; Pierce Biotechnology, Rockford, IL, USA); 25 μg of protein sample was loaded on 13% SDS-polyacrylamide gels. After electrophoresis, gels were electrotransferred onto nitrocellulose filters, and then the filters were blocked with 5% nonfat dried milk in PBT (phosphate-buffered saline with 0.05% Tween 20) and incubated with anti-acK5H2b (Cell Signaling) and anti-H3 (Abcam) antibodies in 5% BSA in PBT. After three washes with PBT, filters were incubated with the corresponding secondary antibody at 1:10000 dilution in 1.5% milk in PBT and developed with Immobilon Western Chemiluminescent HRP substrate (Millipore).

Acknowledgments

Author contributions

FGO, IV, EL, JE, and RS carried out the experimental work, FGO, IV, JMPF, and CLO wrote the paper, IV, XSP, MFF, JMPF, and CLO designed the study and were involved in the analysis and interpretation of the data.

References

Archer SY, Meng S, Shei A, Hodin RA (1998) p21(WAF1) is required for butyrate-mediated growth inhibition of human colon cancer cells. *Proc. Natl. Acad. Sci. U.S.A.* **95**, 6791–6796.

Bergo MO, Gavino B, Ross J, Schmidt WK, Hong C, Kendall LV, Mohr A, Meta M, Genant H, Jiang Y, Wisner ER, Van Bruggen N, Carano RA, Michaelis S, Griffey SM, Young SG (2002) Zmpste24 deficiency in mice causes spontaneous bone fractures, muscle weakness, and a prelamin A processing defect. *Proc. Natl. Acad. Sci. U.S.A* **99**, 13049–13054.

Bickerstaff MC, Botto M, Hutchinson WL, Herbert J, Tennent GA, Bybee A, Mitchell DA, Cook HT, Butler PJ, Walport MJ, Pepys MB (1999) Serum amyloid P component controls chromatin degradation and prevents antinuclear autoimmunity. *Nat. Med.* **5**, 694–697.

Casillas MA Jr, Lopatina N, Andrews LG, Tollefsbol TO (2003) Transcriptional control of the DNA methyltransferases is altered in aging and neoplastically-transformed human fibroblasts. *Mol. Cell. Biochem.* **252**, 33–43.

Chan MW, Wei SH, Wen P, Wang Z, Matei DE, Liu JC, Liyanarachchi S, Brown R, Nephew KP, Yan PS, Huang TH (2005) Hypermethylation of 18S and 28S ribosomal DNAs predicts progression-free survival in patients with ovarian cancer. *Clin. Cancer Res.* **11**, 7376–7383.

Chen ZJ, Pikaard CS (1997) Epigenetic silencing of RNA polymerase I transcription: a role for DNA methylation and histone modification in nucleolar dominance. *Genes Dev.* **11**, 2124–2136.

Christensen BC, Houseman EA, Marsit CJ, Zheng S, Wrensch MR, Wiemels JL, Nelson HH, Karagas MR, Padbury JF, Bueno R, Sugarbaker DJ, Yeh RF, Wiencke JK, Kelsey KT (2009) Aging and environmental exposures alter tissue-specific DNA methylation dependent upon CpG island context. *PLoS Genet.* **5**, e1000602.

Csoka AB, English SB, Simkevich CP, Ginzinger DG, Butte AJ, Schatten GP, Rothman FG, Sedivy JM (2004) Genome-scale expression profiling of Hutchinson-Gilford progeria syndrome reveals widespread transcriptional misregulation leading to mesodermal/mesenchymal defects and accelerated atherosclerosis. *Aging Cell* **3**, 235–243.

De Sandre-Giovannoli A, Bernard R, Cau P, Navarro C, Amiel J, Boccaccio I, Lyonnet S, Stewart CL, Munnich A, Le Merrer M, Levy N (2003) Lamin a truncation in Hutchinson-Gilford progeria. *Science* **300**, 2055.

Dechat T, Pfleghaar K, Sengupta K, Shimi T, Shumaker DK, Solimando L, Goldman RD (2008) Nuclear lamins: major factors in the structural organization and function of the nucleus and chromatin. *Genes Dev.* **22**, 832–853.

Eriksson M, Brown WT, Gordon LB, Glynn MW, Singer J, Scott L, Erdos MR, Robbins CM, Moses TY, Berglund P, Dutra A, Pak E, Durkin S, Csoka AB, Boehnke M, Glover TW, Collins FS (2003) Recurrent de novo point mutations in lamin A cause Hutchinson-Gilford progeria syndrome. *Nature* **423**, 293–298.

Espada J, Varela I, Flores I, Ugalde AP, Cadinanos J, Pendas AM, Stewart CL, Tryggvason K, Blasco MA, Freije JM, Lopez-Otin C (2008) Nuclear envelope defects cause stem cell dysfunction in premature-aging mice. *J. Cell Biol.* **181**, 27–35.

Fraga MF, Uriol E, Borja Diego L, Berdasco M, Esteller M, Canal MJ, Rodriguez R (2002) High-performance capillary electrophoretic method for the quantification of 5-methyl 2′-deoxycytidine in genomic DNA: application to plant, animal and human cancer tissues. *Electrophoresis* **23**, 1677–1681.

Fraga MF, Ballestar E, Villar-Garea A, Boix-Chornet M, Espada J, Schotta G, Bonaldi T, Haydon C, Ropero S, Petrie K, Iyer NG, Perez-Rosado A, Calvo E, Lopez JA, Cano A, Calasanz MJ, Colomer D, Piris MA, Ahn N, Imhof A, Caldas C, Jenuwein T, Esteller M (2005) Loss of acetylation at Lys16 and trimethylation at Lys20 of histone H4 is a common hallmark of human cancer. *Nat. Genet.* **37**, 391–400.

Fuke C, Shimabukuro M, Petronis A, Sugimoto J, Oda T, Miura K, Miyazaki T, Ogura C, Okazaki Y, Jinno Y (2004) Age related changes in 5-methylcytosine content in human peripheral leukocytes and placentas: an HPLC-based study. *Ann. Hum. Genet.* **68**, 196–204.

Gravina S, Vijg J (2010) Epigenetic factors in aging and longevity. *Pflugers Arch.* **459**, 247–258.

Hennekam RC (2006) Hutchinson-Gilford progeria syndrome: review of the phenotype. *Am. J. Med. Genet. A* **140**, 2603–2624.

Issa JP (2003) Age-related epigenetic changes and the immune system. *Clin. Immunol.* **109**, 103–108.

Johnson FB, Marciniak RA, Guarente L (1998) Telomeres, the nucleolus and aging. *Curr. Opin. Cell Biol.* **10**, 332–338.

Liu B, Wang J, Chan KM, Tjia WM, Deng W, Guan X, Huang JD, Li KM, Chau PY, Chen DJ, Pei D, Pendas AM, Cadinanos J, Lopez-Otin C, Tse HF, Hutchison C, Chen J, Cao Y, Cheah KS, Tryggvason K, Zhou Z (2005) Genomic instability in laminopathy-based premature aging. *Nat. Med.* **11**, 780–785.

Maegawa S, Hinkal G, Kim HS, Shen L, Zhang L, Zhang J, Zhang N, Liang S, Donehower LA, Issa JP (2010) Widespread and tissue specific age-related DNA methylation changes in mice. *Genome Res.* **20**, 332–340.

Marino G, Ugalde AP, Salvador-Montoliu N, Varela I, Quiros PM, Cadinanos J, van der Pluijm I, Freije JM, Lopez-Otin C (2008) Premature aging in mice activates a systemic metabolic response involving autophagy induction. *Hum. Mol. Genet.* **17**, 2196–2211.

Matheu A, Klatt P, Serrano M (2005) Regulation of the INK4a/ARF locus by histone deacetylase inhibitors. *J. Biol. Chem.* **280**, 42433–42441.

Merideth MA, Gordon LB, Clauss S, Sachdev V, Smith AC, Perry MB, Brewer CC, Zalewski C, Kim HJ, Solomon B, Brooks BP, Gerber LH, Turner ML, Domingo DL, Hart TC, Graf J, Reynolds JC, Gropman A, Yanovski JA, Gerhard-Herman M, Collins FS, Nabel EG, Cannon III RO, Gahl WA, Introne WJ (2008) Phenotype and course of Hutchinson-Gilford progeria syndrome. *N. Engl. J. Med.* **358**, 592–604.

Navarro CL, Cau P, Levy N (2006) Molecular bases of progeroid syndromes. *Hum. Mol. Genet.* **15** (Spec No. 2), R151–R161.

Oakes CC, Smiraglia DJ, Plass C, Trasler JM, Robaire B (2003) Aging results in hypermethylation of ribosomal DNA in sperm and liver of male rats. *Proc. Natl. Acad. Sci. U.S.A* **100**, 1775–1780.

Olson MO, Dundr M (2005) The moving parts of the nucleolus. *Histochem. Cell Biol.* **123**, 203–216.

Osorio FG, Obaya AJ, Lopez-Otin C, Freije JM (2009) Accelerated ageing: from mechanism to therapy through animal models. *Transgenic Res.* **18**, 7–15.

Pendas AM, Zhou Z, Cadinanos J, Freije JM, Wang J, Hultenby K, Astudillo A, Wernerson A, Rodriguez F, Tryggvason K, Lopez-Otin C (2002) Defective prelamin A processing and muscular and adipocyte alterations in Zmpste24 metalloproteinase-deficient mice. *Nat. Genet.* **31**, 94–99.

Powell MA, Mutch DG, Rader JS, Herzog TJ, Huang TH, Goodfellow PJ (2002) Ribosomal DNA methylation in patients with endometrial carcinoma: an independent prognostic marker. *Cancer* **94**, 2941–2952.

Ramirez CL, Cadinanos J, Varela I, Freije JM, Lopez-Otin C (2007) Human progeroid syndromes, aging and cancer: new genetic and epigenetic insights into old questions. *Cell. Mol. Life Sci.* **64**, 155–170.

Richardson B (2003) Impact of aging on DNA methylation. *Ageing Res. Rev.* **2**, 245–261.

Richon VM, Zhou X, Secrist JP, Cordon-Cardo C, Kelly WK, Drobnjak M, Marks PA (2004) Histone deacetylase inhibitors: assays to assess effectiveness *in vitro* and *in vivo*. *Methods Enzymol.* **376**, 199–205.

Santoro R, Li J, Grummt I (2002) The nucleolar remodeling complex NoRC mediates heterochromatin formation and silencing of ribosomal gene transcription. *Nat. Genet.* **32**, 393–396.

Scaffidi P, Misteli T (2005) Reversal of the cellular phenotype in the premature aging disease Hutchinson-Gilford progeria syndrome. *Nat. Med.* **11**, 440–445.

Scaffidi P, Misteli T (2006) Lamin A-dependent nuclear defects in human aging. *Science* **312**, 1059–1063.

Shahbazian MD, Grunstein M (2007) Functions of site-specific histone acetylation and deacetylation. *Annu. Rev. Biochem.* **76**, 75–100.

Shumaker DK, Dechat T, Kohlmaier A, Adam SA, Bozovsky MR, Erdos MR, Eriksson M, Goldman AE, Khuon S, Collins FS, Jenuwein T, Goldman RD (2006) Mutant nuclear lamin A leads to progressive alterations of epigenetic control in premature aging. *Proc. Natl. Acad. Sci. U.S.A* **103**, 8703–8708.

Shvarts A, Brummelkamp TR, Scheeren F, Koh E, Daley GQ, Spits H, Bernards R (2002) A senescence rescue screen identifies BCL6 as an inhibitor of anti-proliferative p19(ARF)-p53 signaling. *Genes Dev.* **16**, 681–686.

Sinclair DA, Oberdoerffer P (2009) The ageing epigenome: damaged beyond repair? *Ageing Res. Rev.* **8**, 189–198.

Tawa R, Ueno S, Yamamoto K, Yamamoto Y, Sagisaka K, Katakura R, Kayama T, Yoshimoto T, Sakurai H, Ono T (1992) Methylated cytosine level in human liver DNA does not decline in aging process. *Mech. Ageing Dev.* **62**, 255–261.

Thomas S, Mukherjee AB (1996) A longitudinal study of human age-related ribosomal RNA gene activity as detected by silver-stained NORs. *Mech. Ageing Dev.* **92**, 101–109.

Tra J, Kondo T, Lu Q, Kuick R, Hanash S, Richardson B (2002) Infrequent occurrence of age-dependent changes in CpG island methylation as detected by restriction landmark genome scanning. *Mech. Ageing Dev.* **123**, 1487–1503.

Trapnell C, Pachter L, Salzberg SL (2009) TopHat: discovering splice junctions with RNA-Seq. *Bioinformatics* **25**, 1105–1111.

Trapnell C, Williams BA, Pertea G, Mortazavi A, Kwan G, van Baren MJ, Salzberg SL, Wold BJ, Pachter L (2010) Transcript assembly and quantification by RNA-Seq reveals unannotated transcripts and isoform switching during cell differentiation. *Nat. Biotechnol.* **28**, 511–515.

Turner BM, Fellows G (1989) Specific antibodies reveal ordered and cell-cycle-related use of histone-H4 acetylation sites in mammalian cells. *Eur. J. Biochem.* **179**, 131–139.

Varela I, Cadinanos J, Pendas AM, Gutierrez-Fernandez A, Folgueras AR, Sanchez LM, Zhou Z, Rodriguez FJ, Stewart CL, Vega JA, Tryggvason K, Freije JM, Lopez-Otin C (2005) Accelerated ageing in mice deficient in Zmpste24 protease is linked to p53 signalling activation. *Nature* **437**, 564–568.

Varela I, Pereira S, Ugalde AP, Navarro CL, Suarez MF, Cau P, Cadinanos J, Osorio FG, Foray N, Cobo J, de Carlos F, Levy N, Freije JM, Lopez-Otin C (2008) Combined treatment with statins and aminobisphosphonates extends longevity in a mouse model of human premature aging. *Nat. Med.* **14**, 767–772.

Wilhelm BT, Marguerat S, Watt S, Schubert F, Wood V, Goodhead I, Penkett CJ, Rogers J, Bahler J (2008) Dynamic repertoire of a eukaryotic transcriptome surveyed at single-nucleotide resolution. *Nature* **453**, 1239–1243.

Wilson VL, Jones PA (1983) DNA methylation decreases in aging but not in immortal cells. *Science* **220**, 1055–1057.

Supporting Information

Additional supporting information may be found in the online version of this article:

Fig. S1 Differential expression of genes associated with acetylated histone H2B in *Zmpste24*-deficient and control mice. RNA levels corresponding to a selection of genes found to be differentially expressed by ultra-deep RNA sequencing were studied by qRT–PCR with specific Taqman probes. (a) Genes up-regulated in control mice. (b) Genes down-regulated in *Zmpste24*-deficient mice. *$P < 0.05$; **$P < 0.01$; ***$P < 0.001$. Error bars represent SEM.

Table S1 Oligonucleotides used to amplify bisulfite-modified DNA.

Table S2 Genes recurrently enriched in *Zmpste24*$^{+/+}$ samples.

Table S3 Genes recurrently enriched in *Zmpste24*$^{-/-}$ samples.

As a service to our authors and readers, this journal provides supporting information supplied by the authors. Such materials are peer-reviewed and may be re-organized for online delivery, but are not copy-edited or typeset. Technical support issues arising from supporting information (other than missing files) should be addressed to the authors.